

Multiple spin-resolved negative differential resistance and electrically controlled spin-polarization in transition metal-doped [6]cycloparaphenylenes

Yan-Dong Guo^{a,b}, Hong-Li Zeng^{c,*}, Li-Zhi Hu^a, Xiao-Hong Yan^{a,d,*}, Xin-Yi Mou^a,
Mou-Shu Yang^a

^a College of Electronic and Optical Engineering, Nanjing University of Posts and Telecommunications, Nanjing 210046, China

^b Key Laboratory of Radio Frequency and Micro-Nano Electronics of Jiangsu Province, Nanjing 210023, China

^c College of Natural Science, Nanjing University of Posts and Telecommunications, Nanjing 210046, China

^d College of Science, Nanjing University of Aeronautics and Astronautics, Nanjing 210016, China

ARTICLE INFO

Article history:

Received 17 April 2018

Received in revised form 27 June 2018

Accepted 17 July 2018

Available online 19 July 2018

Communicated by R. Wu

Keywords:

Cycloparaphenylene

Spin-polarized transport

Negative differential resistance

Density-functional theory

Nonequilibrium Green's function

ABSTRACT

In structure, a [n]cycloparaphenylene ([n]CPP) molecule is constructed by fully conjugated bent benzenes, i.e., hexangular rings. Based on first-principles calculations, the spin-dependent electronic transport of transition metal-doped CPP, X@[6]cycloparaphenylene (X@[6]CPP) (X = Fe, Co and Ni), contacted with Au electrodes is investigated. (Multiple) negative differential resistance (NDR) is observed for all the doping cases, suggesting it is the intrinsic feature of such systems. Due to the spin dependence of the NDR, electrical switch of the direction of spin polarization for a current is realized. Further analysis shows that it is the suppression of the transmission peaks around the Fermi level as the bias increases that results in the NDR. The suppression is caused by the decay of the local density of states on the scattering region. As electrically controlled spin polarization is a promising area in nanoelectronics, we believe our results would be quite beneficial to the development of spintronic devices.

© 2018 Elsevier B.V. All rights reserved.

1. Introduction

In recent years, spintronics has become a promising field in nanoelectronics [1–3]. Due to the demand of reducing dimensions of electronic devices, lots of attention has been paid to molecular spintronics, where molecules are used as spin transport channels. Up to now, tremendous (spin-related) electronic phenomena have been revealed in molecular systems, such as spin filter effect and negative differential resistance (NDR) [4–10]. Among them, NDR attracts much attention owing to the wide application potentials, e.g., memory, amplification and logic operator [5–11].

Due to the peculiar electrical properties, carbon-based structures are considered to be one of the most promising materials for future nanoelectronic devices [12]. Recently, the synthesis of [n]cycloparaphenylene ([n]CPP) has attracted great interest because of its unique geometry [13–15]. In structure, a [n]CPP molecule is constructed by several fully conjugated bent benzenes, i.e., hexangular rings. For instance, [6]CPP is made up of 6 benzenes [16,17].

For hexangular ring-based carbon structures, great progress has been made in spintronics, especially in graphene and carbon nanotubes [18–20]. To fulfill the gap of their application in molecular spintronics, there is a need to explore the spin-dependent electronic properties in hexangular ring-based molecules. Owing to the geometry, [n]CPP becomes a good candidate. However, unlike zigzag graphene ribbons, there is no zigzag edge on this molecule, so it does not possess spontaneous magnetism. Thus, although much attention has been paid to the synthesis and electronic structure of [n]CPPs, few of them focus on the spin-related electronic transport.

As well known, doping is a useful way to modulate the electronic structure and transport properties in nanomaterials. Furthermore, doping with transition metal could make a system acquire magnetism and exhibit interesting spin-related features [21–29]. In the present work, we investigate the spin-dependent transport of [6]CPP systems doping with transition metals, i.e., X@[6]CPP (X = Fe, Co and Ni), which are contacted with Au electrodes. The study is carried out by density functional theory calculations (DFT) combined with nonequilibrium Green's function (NEGF). It is found that Fe- and Co-doped systems exhibit spin-polarized transport and Ni-doped ones exhibit spin-unpolarized transport. Moreover,

* Corresponding authors.

E-mail addresses: hlzeng@njupt.edu.cn (H.-L. Zeng), yanxh@njupt.edu.cn (X.-H. Yan).

NDR phenomenon is observed in all doping systems (multiple NDRs for some cases), suggesting it is the intrinsic feature of such systems. In Fe- and Co-doped cases, NDR exhibits spin asymmetric dependence. This results in a switch of the direction for the spin polarization of the current, realizing the control of spin polarization through electrical means. Electrically controlled spin polarization is a promising area in nanoelectronics, as compared with conventional magnetic ways, it could reduce the energy consumption and dimensions of the devices [30,31]. We believe our results is quite useful in the development of spintronic devices.

2. Computational method

The calculations are carried out using the Atomistix Toolkit package [32–34], which is based on the combination of DFT and NEGF. We use the mesh cutoff energy of 150 Ry, and $1 \times 1 \times 100$ k -point mesh in the Monkhorst–Pack scheme [35]. The Perdew–Burke–Ernzerhof formulation of the generalized gradient approximation (GGA) to the exchange correlation functional is used [36]. The double-zeta polarized (DZP) basis set of local numerical orbitals is employed in all the calculations. The supercell with sufficient vacuum spaces (more than 10 Å) is chosen to prevent the interactions with adjacent images. To mimic the actual situation, the positions of all atoms in the configurations have been relaxed before the transport calculations and the maximal force is set to be 0.02 eV/Å. According to previous experimental and theoretical studies on related systems, such a kind of carbon-based molecule could remain its structure after contacting with metal electrode, which has been confirmed by the optimization calculations based on density functional theory [37,38]. In the present work, the molecule-electrode distance is optimized by minimizing the total energy of the two-probe system. This contact method has been widely used in the two-probe systems based on metal-molecule-metal configurations [39,40].

In NEGF theory, the current is obtained according to the Landauer–Büttiker formula

$$I(V)_{\uparrow\downarrow} = \frac{2e}{h} \int T(E, V)_{\uparrow\downarrow} [f(E - \mu_L) - f(E - \mu_R)] dE,$$

where $\mu_{L/R}$ is the chemical potential of the left/right electrode, $f(E - \mu_{L/R})$ is the Fermi function of the left/right electrode, and $V = (\mu_L - \mu_R)/e$ is the bias window. In theory, the bias window is defined as the integral window for calculating the current. In the present work, it refers to $[E_F - V/2, E_F + V/2]$, where E_F is the quasi Fermi level of the two-probe system. $T(E, V)_{\uparrow\downarrow}$ is the transmission probability through the system for spin-up/down, which is obtained by (the denotation of spin is omitted)

$$T(E, V) = \text{Tr}[\Gamma_L(E, V)G^R(E, V)\Gamma_R(E, V)G^A(E, V)],$$

where $G^{R/A}(E, V)$ is the retarded/advanced Green's function of the scattering region, and $\Gamma_{L/R}$ is the coupling matrix to the left/right electrode.

3. Results and discussions

In structure, [6]CPP can be considered as a nanohoop consisting of six fully conjugated bent benzenes in the para position, shown in Fig. 1(a). The molecule is saturated with H atoms on the edges to eliminate dangling bonds. In experiment, [6]CPP could be synthesized in at least two ways [16,17]. As we know, there are many ways of doping in such a molecule. Here the CPP molecule is like a cage. Doping the metal atom on the inner site and exposing carbon atoms outside would make the configuration be more inert, compared with that exposing the metal atom outside. It is quite beneficial for the practical application, which would make

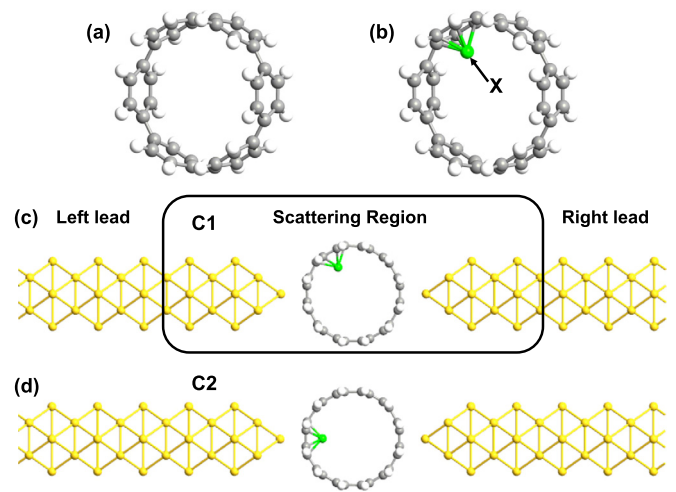


Fig. 1. (Color online.) (a)–(b) The structures of pristine [6]CPP and X@[6]CPP, respectively. X = Fe, Co and Ni. (c)–(d) Geometries of the two-probe Au–X@[6]CPP–Au systems for contact configurations of C1 (c) and C2 (d), respectively.

the nanoelectronic devices possess good stabilization. In addition, previous studies show that, for transition metals, hollow site is more favorable for doping in such a kind of system [41–43]. So, in the present work, we focus on the inner hollow site of the ring to dope with transition metals. Here, we choose Fe, Co and Ni to dope in [6]CPP on the inner hollow site of the ring, shown in Fig. 1(b) (X@[6]CPP, X = Fe, Co and Ni). To mimic the realistic situation, Au nanowire with an atomic tip is used as the electrode to study the transport properties, which is contacted with the molecule on its hollow site. To realize a good contact between the molecule and electrodes, we contact the Au electrodes at the hollow site of the molecule. In a [6]CPP molecule, there are six hexagonal rings. So, there will be totally six two-probe contact configurations. Considering the symmetry of the left and right electrodes, as well as the symmetry of the doping molecule, there is only two independent contact configurations, i.e., C1 and C2, shown in Fig. 1(c) and (d) respectively. Other contact configurations are equivalent to them. For configuration C1, the rings contacted with electrodes are not doped with metal atoms. And for configuration C2, there is a rotation of the molecule compared with that of C1, and the ring doped with metal atom contacts with the left electrode. So, the difference between C1 and C2 is the orientation of the molecule relative to the electrodes.

Fig. 2 shows the total and spin-resolved currents as a function of the bias voltage (I – V curve) for Fe-doped systems (Fe@[6]CPP), where the left and right panels are for the configurations of C1 and C2 respectively. For configuration C1, one easily finds there is a threshold at the bias of 0.8 V. The total current increases only a little when the bias is smaller than 0.8 V, see Fig. 2(a). Actually, there is a NDR in the bias region of [0.4, 0.6] V, but not obvious. When V_b is larger than 0.8 V, the current increases almost linearly with V_b . However, when V_b exceeds 1.7 V, the current decreases with the further increase of bias and the NDR behavior appears again.

From the spin-resolved I – V curves in Fig. 2(b), one finds the spin-up and down currents show the same variation trend as the total one in Fig. 2(a). But they are not the same between spin-up and down, so the current becomes spin-polarized. For the spin-up current, there are two main NDR regions, i.e., [0.4, 0.6] V and [1.7, 2.0] V (note there is an oscillation around 1.9 V). However, for spin-down one, there is only one NDR region around 1.8 V, and there is none in the lower bias range of [0.4, 0.6] V. As the total current is the sum of the spin-up and down currents, the NDRs

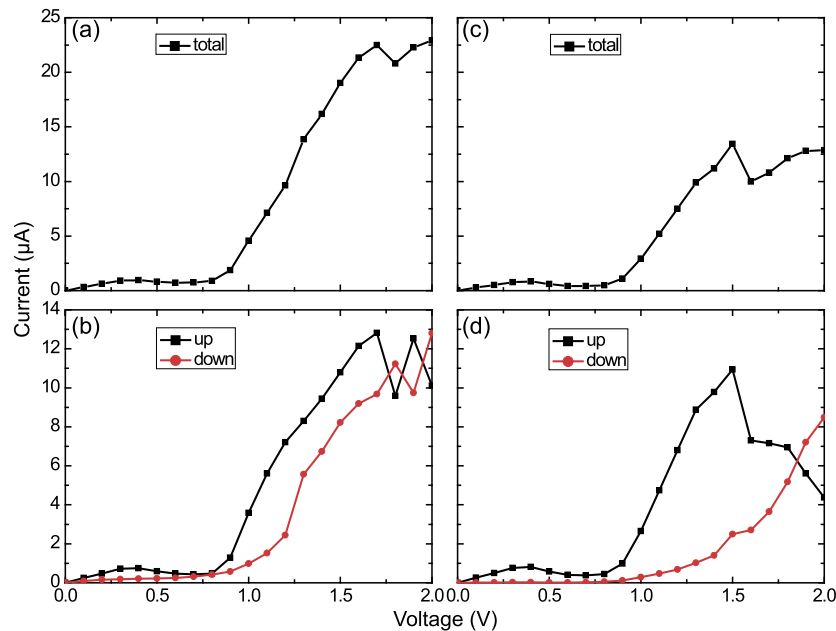


Fig. 2. (Color online.) The current as a function of the applied bias for the Au-Fe@[6]CPP-Au systems. (a)–(b) The total and spin resolved currents of contact configuration C1, respectively. (c)–(d) The total and spin resolved currents for contact configuration C2, respectively.

in total current are contributed to by those of spin-resolved ones, although in some bias regions NDR does not appear for spin-down.

For the contact configuration C2, the total current has the same variation trend as that of C1, see Fig. 2(c). The threshold still locates at 0.8 V. When bias is larger than 0.8 V, the current goes up as the bias increases, but it is smaller than that of C1 in the same bias range. Apparently, the two NDRs remain, although the latter one moves to the bias range of [1.5, 1.6] V. For the spin-up I–V curve, it has almost the same variation trend as the total current. But for the latter NDR, it has a more obvious NDR behavior in a larger bias range of [1.5, 2.0] V. While, for the spin-down component, there is no NDR in the whole bias range. Such a spin-dependent NDR behavior may be used in spin-related devices, e.g., logic operator and data storage. Below the threshold bias of 0.8 V, the current is almost zero, and above that it increases gradually.

Interestingly, in the bias range of [1.5, 2.0] V, the spin-up and down currents exhibit opposite variation trend, i.e., one goes up and another goes down. This results in a cross around 1.85 V. When the bias is below the cross point, [0, 1.85] V, the spin-up current is larger than the spin-down one, so the total current is spin-up polarized. But above that point, it is the spin-down current that dominates the transmission, and the total current is spin-down polarized. In other words, there is a switch of the direction for the current's spin polarization at the cross point. We here define the spin polarization of a current as $[(I_{up} - I_{down}) / (I_{up} + I_{down})] \times 100\%$. Note that this is an electrically controlled switch. Comparing with magnetic means, electrical methods could largely reduce the energy consumption and dimensions (eliminating the use of ferromagnetic contacts) of integrated devices, which has attracted much attention [31]. And it could be used in a wide range of applications, e.g., logic operators and data storage. Apparently, the switch of spin polarization here is induced by the spin-dependent NDR. The origin of NDR will be discussed in the following.

For Co-doped systems, the total and spin-resolved I–V curves are shown in Fig. 3. In the high-bias range, NDR behavior appears again in both C1 and C2 configurations, but only in the spin-up component, not in the spin-down one, see Fig. 3(b) and (d). Such a spin-dependent NDR behavior likes that of the Fe-doped case (C2 configuration). However, in the low-bias range of [0.4, 0.8] V,

NDR emerges in both spin-up and down components, for both C1 and C2 configurations. This is quite different from that of Fe cases, where only a minor NDR appears in spin-up component. Apparently, the contact configuration between electrodes and molecule has little effect on the I–V and NDR behaviors in Co-doped systems, see Fig. 3(b) and (d). This robustness is actually beneficial to the practical fabrication of a device. Moreover, the realization of both spin-independent (low-bias case) and spin-dependent (high-bias case) NDRs in a single molecule could be used for quite interesting applications. For the total current, there are two NDRs in C1 or C2 configuration. But the high-bias NDR is less obvious than the low-bias one, as the spin-down current exhibits no NDR in the high biases. Besides, there is also crosses between spin-up and down I–V curves in Co-doped systems. But the spin-up and down currents are close to each other, so the spin-polarization of the total current is not as large as that of Fe-doped systems.

For the Ni-doped case, it is quite different from the Fe- and Co-systems. Fig. 4 shows the I–V curves of it. For the total current, the threshold feature at the bias of 0.8 V preserves. But only one obvious NDR appears, which locates within the high bias in C2 configuration, see Fig. 4(c). However, for the spin-resolved currents, there are no difference between spin-up and down ones. They exactly coincide with each other and present completely spin-unpolarized current, not like that of Fe- or Co-doped systems. Thus, the vibration trend of the spin-resolved currents is the same as the total one. Although the spin-independent feature is quite different from Fe- and Co-doped systems, the appearance of NDR suggests it is the intrinsic feature of this CPP molecule. In the following, we will discuss the underlying mechanism on the decay of spin polarization in Ni-doped systems.

To further understand the NDR phenomenon, we calculate the transmission spectra of the two-probe systems. Taking the Fe-doped C2 system as an example, we plot the transmission spectra for the spin-up component at the biases of 1.5, 1.8 and 2.0 V, shown in Fig. 5(a)–(c) respectively. In theory, the current of a system is obtained through the Landauer–Büttiker formula. According to it, by integrating the transmission coefficient in the bias window, we can obtain the current of the system. For clarity, in Fig. 5, each bias window is denoted by two blue solid lines. At the bias of 1.5 V, Fig. 5(a) shows there are two transmission peaks lying in

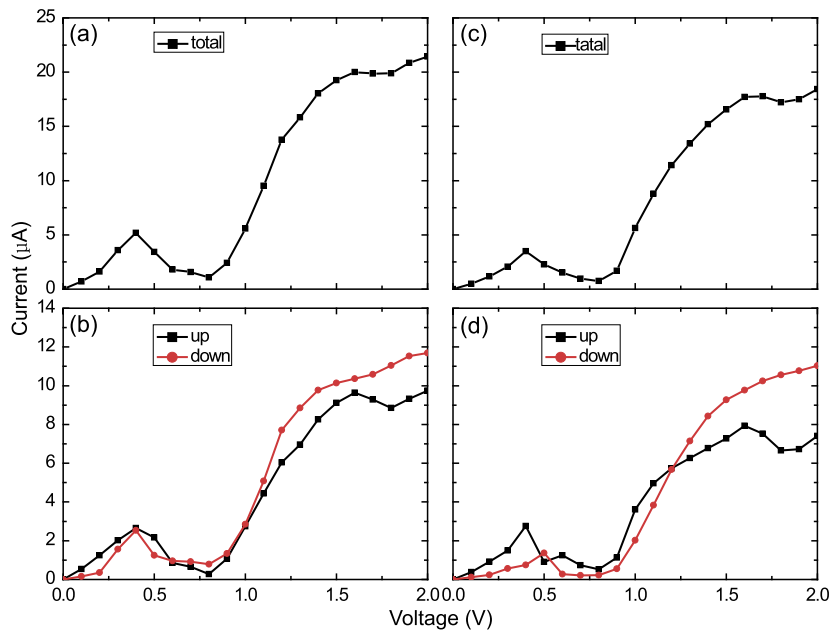


Fig. 3. (Color online.) The current as a function of the applied bias for the Au-Co@[6]CPP-Au systems. (a)–(b) The total and spin resolved currents of contact configuration C1, respectively. (c)–(d) The total and spin resolved currents of contact configuration C2, respectively.

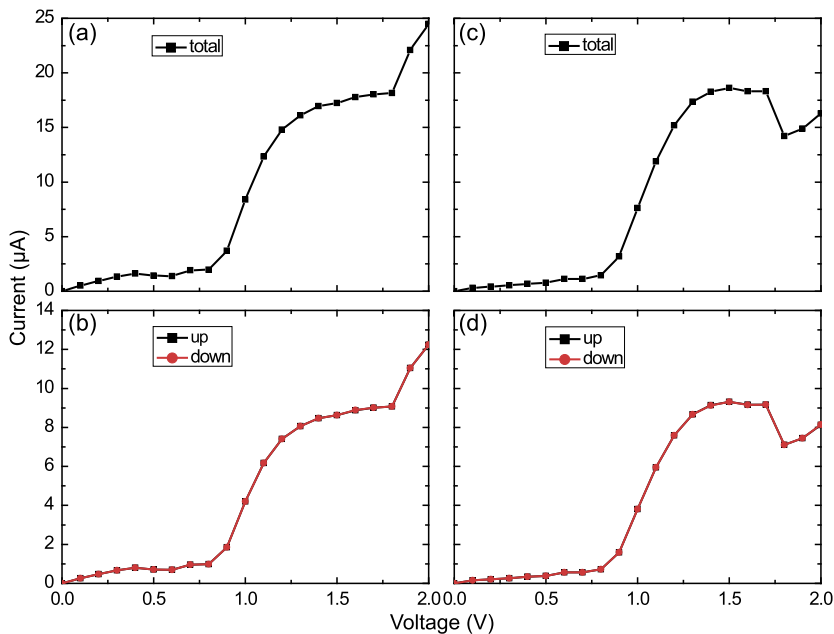


Fig. 4. (Color online.) The current as a function of the applied bias for the Au-Ni@[6]CPP-Au systems. (a)–(b) The total and spin resolved currents of contact configuration C1, respectively. (c)–(d) The total and spin resolved currents of contact configuration C2, respectively.

the bias window, which attributes to a large current for this bias. When the bias increases to 1.8 V, the height of the left peak remains almost unchanged. But it shifts slightly to the lower biases, even out of the former integral window of 1.5 V. Fortunately, the bias window becomes wider when the bias increases to 1.8 V, so the left peak still locates in the corresponding integral window and contributes to the current. However, the right peak changes quite a lot. It almost disappears when $V_b = 1.8$ V. Thus, although the bias window becomes wider, the total integral area gets smaller. This results in a great decrease of the current. Furthermore, when the bias increases to 2.0 V, the left peak also decreases quite a lot. Finally, there is almost no strong transmission peak. As a result, the current decreases remarkably and the NDR appears in this bias range, i.e., [1.5, 2.0] V.

To figure out the origin of the peaks which are suppressed in transmission spectra in Fig. 5, we calculate the local density of states (LDOS) for the two-probe systems, shown in Fig. 6. The energies of the LDOS are chosen to be the peak-point energies, i.e., $E = -0.67$ (0.62), -0.72 (0.62) and -0.68 (0.62) eV for the biases of $V = 1.5$, 1.8 and 2.0 V respectively, which are denoted by black dotted lines in Fig. 5. From Fig. 6(a1) and (b1), one can see clearly that when the bias is 1.5 V, the LDOS at $E = -0.67$ and -0.72 eV is fully delocalized throughout the whole system, suggesting that the conduction channel can make a large contribution to the current. As a consequence, a transmission peak appears at the $E = -0.67$ and 0.62 eV for the bias of 1.5 V, as shown in Fig. 5(a). However, in Fig. 6(a2) and (b2), it can be observed that when the bias becomes 1.8 V, although the LDOS at $E = -0.72$ eV (a2) is fully delocal-

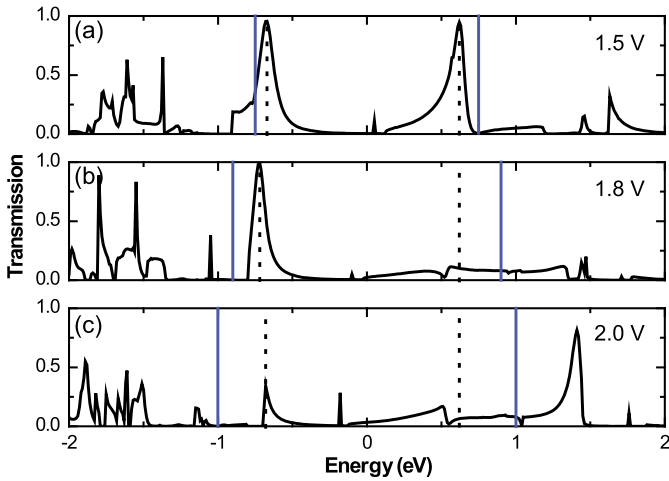


Fig. 5. (Color online.) (a)–(c) The spin-up transmission spectra for configuration C2 of Au-Fe@[6]CPP-Au system under bias voltages of 1.5, 1.8 and 2.0 V, respectively. The Fermi level is set to be $E_F = 0$ and the solid blue lines indicate the bias window. The dashed line indicates the energy position of the transmission peak near E_F . Note that the right dashed line in (b) or (c) is in the same energy position as that in (a), as the peak disappears in (b) and (c).

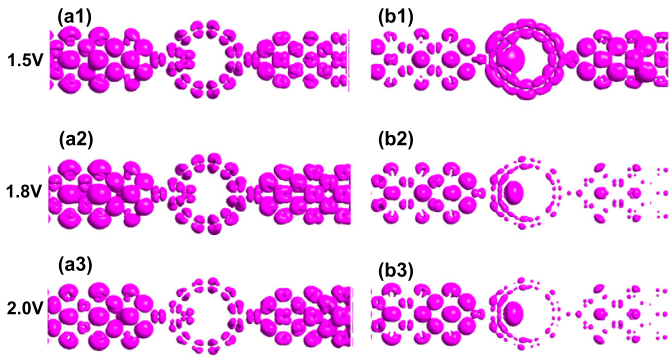


Fig. 6. (Color online.) The local density of states under different bias voltages for configuration C2 of Au-Fe@[6]CPP-Au system. (a1)–(a3) LDOS at $E = -0.67$, -0.72 and -0.68 eV under the bias voltages of 1.5, 1.8, and 2.0 V, respectively. They correspond to the left dashed lines in Fig. 5(a)–(c) respectively. (b1)–(b3) LDOS at $E = 0.62$ eV under the bias voltages of 1.5, 1.8, and 2.0 V, respectively. They correspond to the right dashed lines in Fig. 5(a)–(c) respectively.

ized on the whole structure, the LDOS at $E = -0.62$ eV (b2) is not delocalized throughout the whole configuration. On the right lead and the contact region between the right lead and the molecule, the LDOS decays a lot. As a result, the conduction channel will be suppressed, and the transmission peak is lowered down and almost disappears. Therefore, the current at the bias of 1.8 V becomes smaller than that of 1.5 V. When the bias increases to 2.0 V, the distribution of LDOS on the molecule at $E = -0.68$ eV also becomes weakened, see Fig. 6(a3). This results in the suppression of the left peak and accounts for the NDR.

Note there is an oscillation behavior around 1.9 V for spin-up current in the configuration C1 of Au-Fe@[6]CPP-Au, shown in Fig. 2(b). To figure out the underlying mechanism, we calculate the corresponding transmission spectra under the biases of 1.7, 1.8, 1.9 and 2.0 V (not shown). It is found that the oscillation is caused by the decrease of the transmission peak around -0.70 eV under the biases of 1.8 and 2.0 V. Further analysis shows that, it is the decay of the states around -0.70 eV in the scattering region induced by the bias change that triggers the decrease of transmission at 1.8 and 2.0 V. The decay makes the LDOS non-continuous throughout the two-probe system (not shown), and do not contribute to the current. In practical applications, such an oscillation could be avoided by confining the operating bias range.

Table 1

The Mulliken population of metal atom X in isolated X@[6]CPP (X=Fe, Co and Ni), which is not contacted with Au electrodes, for spin-up, spin-down and their difference (up-down, i.e., the magnetic moment). The unit of magnetic moment is μ_B .

Configuration	↑	↓	↑ − ↓
Fe@[6]CPP	5.018	2.730	2.288
Co@[6]CPP	4.960	3.776	1.184
Ni@[6]CPP	4.834	4.834	0

Table 2

The Mulliken population of metal atom X in Au-X@[6]CPP-Au (X=Fe, Co and Ni) for spin-up, spin-down and their difference (up-down, i.e., the magnetic moment). The unit of magnetic moment is μ_B .

Configuration	C1			C2		
	↑	↓	↑ − ↓	↑	↓	↑ − ↓
Fe@[6]CPP	5.020	2.735	2.285	5.052	2.702	2.350
Co@[6]CPP	4.994	3.732	1.262	5.012	3.716	1.296
Ni@[6]CPP	4.835	4.832	0.003	4.835	4.833	0.002

To gain insight into the mechanism of the spin-dependent transport, especially the difference of spin-polarization between different doping cases, we calculate the Mulliken population of the X atom in the isolated X@[6]CPP molecule, which is not contacted with the electrodes. Table 1 shows the Mulliken population of it for spin-up, spin-down and their difference, i.e., the magnetic moment. One finds the magnetic moment of the Fe or Co atoms is quite large in the isolated molecule, i.e., 2.288 and 1.184 μ_B respectively. Apparently, it is these non-zero magnetic moments in X@[6]CPP that result in the spin-polarized I-V curves for Fe- and Co-doped systems. However, for Ni-doped system, the magnetic moment is zero. In former studies, it has been reported that Ni-doped system tends to quench the magnetism compared with Fe- and Co-doped ones [44]. Thus, for Fe-, Co- and Ni-doped systems, it is the non-zero/zero magnetic moment of the molecule that triggers the spin-polarized/unpolarized transport. To confirm that in the two-probe system, we calculate the Mulliken population of the two-probe Au-X@[6]CPP-Au systems. The results are shown in Table 2. As the encapsulated transition metal atom is the only source of the magnetic moment in the whole two-probe system, only the Mulliken population of this atom is presented. From Table 2, one finds the magnetic moment is very large for Fe- and Co-doped systems, but for Ni-doped ones they are almost zero. This is consistent with the that of the isolated doping molecules, suggesting the electrodes have little effect on the magnetic moment of such a molecule. In other words, it shows good robustness to the electrodes, which is useful to the practical applications.

4. Conclusion

In summary, by applying first principles calculations, the spin-dependent transport of [6]CPP system doping with transition metals, contacted with Au electrodes, i.e., Au-X@[6]CPP-Au (X=Fe, Co and Ni), are investigated. (Multiple) NDR behavior is observed for all the doping cases, suggesting it is the intrinsic feature of such systems. In Fe- and Co-doped cases, the NDR is spin-dependent, and the switch of the direction for the spin polarization of the current is realized. Such an electrically controlled spin polarization is quite useful for the development of spintronic devices. Further analysis shows it is suppression of the transmission peaks around E_F as the bias increases that results in the NDR. And the suppression is caused by the decay of the LDOS on the molecule and on the right electrode-molecule contact regions. Moreover, we also investigate the Mulliken population of doping metal atom, and find Fe- and Co-doped systems exhibit large magnetic moment whereas Ni-doped one exhibit zero magnetic moment, which

accounts for their spin-polarized/unpolarized transmission. Our results may throw light on the development of molecular spintronics.

Acknowledgements

This work is supported by the National Natural Science Foundation of China (NSFC11504178 and NSFC11705097), the Natural Science Foundation of Jiangsu Province (BK20150825 and BK20170895), the Scientific Research Foundation of Nanjing University of Posts and Telecommunications (NY217013 and NY214151), and Natural Science Found for Colleges and Universities in Jiangsu Province (17KJB140015).

References

- [1] Y. Ding, Y. Wang, Electronic structures of zigzag silicene nanoribbons with asymmetric sp²–sp³ edges, *Appl. Phys. Lett.* 102 (2013) 143115.
- [2] S. Wolf, D. Awschalom, R. Buhrman, J. Daughton, S. Von Molnar, M. Roukes, A.Y. Chtchelkanova, D. Treger, Spintronics: a spin-based electronics vision for the future, *Science* 294 (2001) 1488.
- [3] N.A. Zimbovskaya, M.R. Pederson, Electron transport through molecular junctions, *Phys. Rep.* 509 (2011) 1.
- [4] I. Lekshmi, G. Berera, Y. Afsar, G. Miao, T. Nagahama, T. Santos, J. Moodera, Controlled synthesis and characterization of Ag₂S films with varied microstructures and its role as asymmetric barrier layer in trilayer junctions with dissimilar electrodes, *J. Appl. Phys.* 103 (2008) 093719.
- [5] J. Chen, M. Reed, A. Rawlett, J. Tour, Large on-off ratios and negative differential resistance in a molecular electronic device, *Science* 286 (1999) 1550.
- [6] J. Chen, W. Wang, M. Reed, A. Rawlett, D. Price, J. Tour, Room-temperature negative differential resistance in nanoscale molecular junctions, *Appl. Phys. Lett.* 77 (2000) 1224.
- [7] M. Di Ventra, S. Pantelides, N. Lang, First-principles calculation of transport properties of a molecular device, *Phys. Rev. Lett.* 84 (2000) 979.
- [8] W.Y. Kim, S. Kwon, K.S. Kim, Negative differential resistance of carbon nanotube electrodes with asymmetric coupling phenomena, *Phys. Rev. B* 76 (2007) 033415.
- [9] M.-Q. Long, K.-Q. Chen, L. Wang, B. Zou, Z. Shuai, Negative differential resistance induced by intermolecular interaction in a bimolecular device, *Appl. Phys. Lett.* 91 (2007) 233512.
- [10] L. Chen, Z. Hu, A. Zhao, B. Wang, Y. Luo, J. Yang, J. Hou, Mechanism for negative differential resistance in molecular electronic devices: local orbital symmetry matching, *Phys. Rev. Lett.* 99 (2007) 146803.
- [11] L. Hu, Y. Guo, X. Yan, H. Zeng, J. Zhou, Electronic transport properties in [n]cycloparaphenylenes molecular devices, *Phys. Lett. A* 381 (2017) 2107.
- [12] P. Avouris, Z. Chen, V. Perebeinos, Carbon-based electronics, *Nat. Nanotechnol.* 2 (2007) 605.
- [13] R. Jasti, C.R. Bertozzi, Progress and challenges for the bottom-up synthesis of carbon nanotubes with discrete chirality, *Chem. Phys. Lett.* 494 (2010) 1.
- [14] E.S. Hirst, R. Jasti, Bending benzene: syntheses of [n]cycloparaphenylenes, *J. Org. Chem.* 77 (2012) 10473.
- [15] H. Omachi, Y. Segawa, K. Itami, Synthesis of cycloparaphenylenes and related carbon nanorings: a step toward the controlled synthesis of carbon nanotubes, *Acc. Chem. Res.* 45 (2012) 1378.
- [16] E. Kayahara, V.K. Patel, J. Xia, R. Jasti, S. Yamago, Selective and gram-scale synthesis of [6]cycloparaphenylene, *Synlett* 26 (2015) 1615.
- [17] J. Xia, R. Jasti, Synthesis, characterization, and crystal structure of [6]cycloparaphenylene, *Angew. Chem., Int. Ed. Engl.* 51 (2012) 2474.
- [18] W. Han, R.K. Kawakami, M. Gmitra, J. Fabian, Graphene spintronics, *Nat. Nanotechnol.* 9 (2014) 794.
- [19] S. Roche, J. Åkerman, B. Beschoten, J.-C. Charlier, M. Chshiev, S.P. Dash, B. Dlubak, J. Fabian, A. Fert, M. Guimarães, et al., Graphene spintronics: the European flagship perspective, *2D Mater.* 2 (2015) 030202.
- [20] H. Santos, A. Latgé, J. Alvarellos, L. Chico, All-electrical production of spin-polarized currents in carbon nanotubes: Rashba spin-orbit interaction, *Phys. Rev. B* 93 (2016) 165424.
- [21] M. Manadé, F. Viñes, F. Illas, Transition metal adatoms on graphene: a systematic density functional study, *Carbon* 95 (2015) 525.
- [22] J. Hu, R. Wu, Giant magnetic anisotropy of transition-metal dimers on defected graphene, *Nano Lett.* 14 (2014) 1853.
- [23] T. Alonso-Lanza, A. Ayuela, F. Aguilera-Granja, Substitutional 4d and 5d impurities in graphene, *Phys. Chem. Chem. Phys.* 18 (2016) 21913.
- [24] J. Vejpravova, B. Pacakova, M. Kalbac, Magnetic impurities in single-walled carbon nanotubes and graphene: a review, *Analyst* 141 (2016) 2639.
- [25] J. Pan, S. Du, Y. Zhang, L. Pan, Y. Zhang, H.-J. Gao, S.T. Pantelides, Ferromagnetism and perfect spin filtering in transition-metal-doped graphyne nanoribbons, *Phys. Rev. B* 92 (2015) 205429.
- [26] C.-K. Yang, J. Zhao, J.P. Lu, Magnetism of transition-metal/carbon-nanotube hybrid structures, *Phys. Rev. Lett.* 90 (2003) 257203.
- [27] A.K. Singh, T.M. Briere, V. Kumar, Y. Kawazoe, Magnetism in transition-metal-doped silicon nanotubes, *Phys. Rev. Lett.* 91 (2003) 146802.
- [28] E. Durgun, S. Ciraci, Spin-dependent electronic structure of transition-metal atomic chains adsorbed on single-wall carbon nanotubes, *Phys. Rev. B* 74 (2006) 125404.
- [29] L. Kong, J.R. Chelikowsky, Transport properties of transition-metal-encapsulated Si cages, *Phys. Rev. B* 77 (2008) 073401.
- [30] Y.-D. Guo, X.-H. Yan, Y. Xiao, Electrical control of the spin polarization of a current in pure-carbon systems based on partially hydrogenated graphene nanoribbon, *J. Appl. Phys.* 113 (2013) 244302.
- [31] C. Chappert, A. Fert, F.N. Van Dau, The emergence of spin electronics in data storage, *Nat. Mater.* 6 (2007) 813.
- [32] Quantumwise A/S, <http://www.quantumwise.com/>.
- [33] M. Brandbyge, J.-L. Mozos, P. Ordejón, J. Taylor, K. Stokbro, Density-functional method for nonequilibrium electron transport, *Phys. Rev. B* 65 (2002) 165401.
- [34] J. Taylor, H. Guo, J. Wang, Ab initio modeling of quantum transport properties of molecular electronic devices, *Phys. Rev. B* 63 (2001) 245407.
- [35] H.J. Monkhorst, J.D. Pack, Special points for Brillouin-zone integrations, *Phys. Rev. B* 13 (1976) 5188.
- [36] J.P. Perdew, K. Burke, M. Ernzerhof, Generalized gradient approximation made simple, *Phys. Rev. Lett.* 77 (1996) 3865.
- [37] G. Schull, T. Frederiksen, A. Arnau, D. Sánchez-Portal, R. Berndt, Atomic-scale engineering of electrodes for single-molecule contacts, *Nat. Nanotechnol.* 6 (2011) 23.
- [38] X.-J. Zhang, M.-Q. Long, K.-Q. Chen, Z. Shuai, Q. Wan, B. Zou, Y. Zhang, Electronic transport properties in doped C₆₀ molecular devices, *Appl. Phys. Lett.* 94 (2009) 073503.
- [39] H. Hao, X. Zheng, L. Song, R. Wang, Z. Zeng, Electrostatic spin crossover in a molecular junction of a single-molecule magnet Fe₂, *Phys. Rev. Lett.* 108 (2012) 017202.
- [40] H. Hao, X. Zheng, Z. Dai, Z. Zeng, Spin-filtering transport and switching effect of MnCu single-molecule magnet, *Appl. Phys. Lett.* 96 (2010) 192112.
- [41] H. Valencia, A. Gil, G. Frapper, Trends in the adsorption of 3d transition metal atoms onto graphene and nanotube surfaces: a DFT study and molecular orbital analysis, *J. Phys. Chem. C* 114 (2010) 14141–14153.
- [42] Y. Yagi, T.M. Briere, M.H. Sluiter, V. Kumar, A.A. Farajian, Y. Kawazoe, Stable geometries and magnetic properties of single-walled carbon nanotubes doped with 3d transition metals: a first-principles study, *Phys. Rev. B* 69 (2004) 075414.
- [43] Y. Mao, J. Yuan, J. Zhong, Density functional calculation of transition metal adatom adsorption on graphene, *J. Phys. Condens. Matter* 20 (2008) 115209.
- [44] W. Wang, Y.-D. Guo, X.-H. Yan, The spin-dependent transport of transition metal encapsulated B₄₀ fullerene, *RSC Adv.* 6 (2016) 40155.